

El Niño-induced tropical droughts in climate change projections

by

Caio A. S. Coelho¹

Centro de Previsão de Tempo e Estudos Climáticos (CPTEC)
Instituto Nacional de Pesquisas Espaciais (INPE)

and

Lisa Goddard

International Research Institute for Climate and Society (IRI)
The Earth Institute at Columbia University

Submitted to Journal of Climate, April 2009

¹ *Corresponding author address:* Caio Coelho, Centro de Previsão de Tempo e Estudos Climáticos (CPTEC), Instituto Nacional de Pesquisas Espaciais (INPE), Rodovia Presidente Dutra, KM 40, SP-RJ, 12630-000, Cachoeira Paulista, SP, Brazil
E-mail: caio.coelho@cptec.inpe.br

Abstract

El Niño brings widespread drought (i.e. precipitation deficit) to the tropics. Stronger or more frequent El Niño events in the future and/or their intersection with local changes in the mean climate towards a future with reduced precipitation would exacerbate drought risk in highly vulnerable tropical areas. Projected changes in El Niño characteristics and associated teleconnections are investigated between the 20th and 21st centuries. For climate change models that reproduce realistic oceanic variability of the El Niño-Southern Oscillation (ENSO) phenomenon, results suggest no robust changes in the strength or frequency of El Niño events. These models exhibit realistic patterns, magnitude, and spatial extent of El Niño-induced drought patterns in the 20th century, and the teleconnections are not projected to change in the 21st century; although a possible slight reduction in the spatial extent of droughts is indicated over the tropics as a whole. All model groups investigated show similar changes in mean precipitation for the end of the 21st century, with increased precipitation projected between 10°S and 10°N, independent of the ability of the models to replicate ENSO variability. These results suggest separability between climate change and ENSO-like climate variability in the tropics. As El Niño induced precipitation drought patterns are not projected to change, the observed 20th century variability is used in combination with model projected changes in mean precipitation for assessing year-to-year drought risk in the 21st century. Results suggest more locally consistent changes in regional drought risk among models with good fidelity in reproducing ENSO variability.

1. Introduction

The majority of drought related hazards and the attendant economic losses and mortality risks reside in the tropics (Dilley et al. 2005). Changes in climate variability, including more frequent and damaging extreme events such as drought, is one of many anticipated impacts of climate change. Estimating how climate variability may change in a warmer world, and how that variability intersects with more slowly evolving climate change is vitally important to climate risk management and adaptation efforts.

El Niño plays the largest role in tropical drought occurrence. For a substantial fraction of the tropics, severe droughts in the meteorological sense (i.e. precipitation deficit) develop preferentially during El Niño events (Lyon 2004). Further, the severity and extent of tropical droughts exhibits a fairly linear relationship to the strength of El Niño events (Lyon 2004). The possibility of increases in the strength or frequency of El Niño events in a warmer future climate have clear negative societal implications for many of the already vulnerable tropical land areas.

Numerous uncertainties surround El Niño and climate change in coupled general circulation models (CGCMs). First, although the latest models developed for the 2007 Intergovernmental Panel on Climate Change (IPCC) Fourth Assessment Report – the so-called Coupled Model Intercomparison Project-3 (CMIP3) models – have improved their representation of ENSO characteristics relative to their predecessors (AchutaRao and Sperber 2006), representations of El Niño-Southern Oscillation (ENSO) variability remain imperfect. Second, it has been suggested that the CMIP3 models disagree on whether El Niño events will become stronger or more frequent, subject to increasing greenhouse gasses (e.g. Meehl et al, 2007, cf. Figure 10.16). Looking at patterns of sea level pressure associated with ENSO, van Oldenborgh et al. (2005a) found that the CMIP3 models disagreed on whether the variance of indices, or time-series, associated with those

patterns would increase or decrease by the end of the 21st century, and stated that in the cases where significant changes did exist they were of the same order as the observed 1866-2004 variance in the Southern Oscillation Index (SOI). Merryfield (2006) examined the variances of principal component time-series of the leading Empirical Orthogonal Function (EOF) of tropical Pacific monthly sea surface temperature (SST) anomalies, representative of ENSO, from double carbon dioxide climate simulations compared to pre-industrial climate simulations, and based on a *t* test, determined whether the differences between the two simulations lay significantly outside of the range set by several century-long pre-industrial cases in each model. Four of the fifteen models examined exhibited differences that exceeded the 5% confidence level, but half of those showed increased amplitude in ENSO variability and the other half showed decreased amplitude. However, this measure may incorporate both spatial and temporal changes within the tropical Pacific that could cancel each other. The conclusion from these studies as well as others is that no firm projection about the future behavior of El Niño variability can be made because the models disagree.

Also discussed in the context of climate change is whether the mean state of the tropical Pacific will come to look more El Niño-like or La Niña-like. This phrasing of mean state change implicitly suggests that the mean tropical climate will as well move towards conditions realized in those phases of ENSO. Climate change models do not agree on whether the spatial pattern of tropical SST changes will resemble El Niño, although according to some studies there may be a slightly greater likelihood for a more El Niño-like future than La Niña-like future (e.g. Collins et al. 2005). This constitutes a third aspect of uncertainty related to El Niño and climate change. Studies supporting a more La Niña-like future base their arguments primarily on ocean mechanisms, while those suggesting a more El Niño-like future have arguments focused on atmospheric mechanisms. Vecchi et al. (2008) suggest that the particular ENSO-like tendency of a model depends on the

relative role of ocean versus atmosphere in the tropical Pacific response to increasing greenhouse gasses. The more La Niña-like response arises from the “ocean thermostat” mechanism (Clement et al. 1996) in which eastern equatorial Pacific upwelling reduces ocean surface warming from increased longwave radiative forcing, thus strengthening the zonal temperature gradient between eastern and western Pacific. The more El Niño-like response follows from a weakening of the Pacific Walker Circulation as precipitation efficiency increases in a warmer, moister world. Such weakening leads to a reduction in the easterlies in the equatorial Pacific, which results in a reduction in the equatorial Pacific east-west SST gradient. Simplifications in ocean mixed layer dynamics common in the current generation of coupled models is likely to be responsible for the relatively weak role of ocean dynamics and thus a greater tendency towards an El Niño-like mean state in the future (Vecchi et al. 2008).

Much this concern over change in the tropical Pacific mean state and its variability arises from the expected impact those changes will have on the climate. Potentially, similar physical mechanisms lead to tropical drying/drought associated with El Niño events and climate change (Neelin et al. 2003). How will the teleconnections observed during El Niño, and in particular tropical droughts, change in the future? In a relative sense, even if ENSO variability were to remain constant, will changes in the mean state modify the teleconnections? Or, in an absolute sense, how will changes in the tropical Pacific mean state intersect with El Niño teleconnections to modify the risk of drought? Sterl et al. (2007) found little evidence for changes in the strength of ENSO atmospheric teleconnections in the 21st century. This study focusses on the precipitation signature of these teleconnections and how they will be realized in the future given the possible changes in the mean state. We investigate the extent to which precipitation changes, particularly the negative changes related to precipitation deficit, interact or intersect with ENSO variability. Studies have examined how ENSO itself may change, and others have looked at regional precipitation changes, but little

has been done on how ENSO teleconnections

– particularly El Niño-induced drought patterns – together with projected precipitation changes in the tropics can inform the changing risk of drought conditions.

This study first evaluates the patterns, magnitude, and spatial extent of El Niño-induced tropical droughts during a control period in the 20th century in climate simulations, which have realistic evolution of greenhouse gasses. Next it examines the projected changes in the characteristics of El Niño, and in the strength of the identified patterns of El Niño-induced tropical drought in the 21st century. Finally, the patterns of mean precipitation changes are examined to assess whether those changes exacerbate or ameliorate the risk of El Niño-induced drought conditions in the 21st century. The use of the term drought in this study is the simple meteorological definition of precipitation deficits. Clearly, as the climate warms, and the atmospheric evaporative demand increases, water availability will decrease even if precipitation totals remain constant (e.g. Wang 2005; Easterling et al. 2007; McCabe and Wolock 2007). Temperature changes in the tropics are likely to be smaller than the global average and will be much more spatially homogenous than mean precipitation changes. Previous studies provided comprehensive analysis of agricultural (Wang 2005) and hydrological (Nohra et al. 2006; Hoerling and Eischeid 2007) droughts in CMIP3 simulations. The investigation performed here complements these previous studies focusing on meteorological droughts in CMIP3 simulations during El Niño events. The interest here is to assess:

- Projected changes in El Niño magnitude and frequency, relative to the 20th century characteristics of El Niño variability
- Changes in El Niño-induced tropical teleconnections in the 21st century relative to those in the 20th century
- The manner in which El Niño-induced tropical teleconnections intersect with 21st century precipitation change

The manuscript is structured as follows. Section 2 describes the datasets and approach used in the investigation. Section 3 presents an analysis of model projected changes in El Niño itself between the 20th and 21st Centuries and also examines the ability of the coupled models to simulate tropical teleconnections associated with El Niño variability during the 20th century. Sections 4 and 5 examine how ENSO-induced drought patterns change in the 21st century and how such patterns can be combined with projected mean precipitation changes for estimating El Niño-induced drought risk in the 21st century. Section 6 concludes the manuscript with a summary and discussion of the findings.

2. Datasets and investigation approach

El Niño precipitation teleconnections are reasonably well reproduced by seasonal climate models (van Oldenborgh et al. 2005b; Coelho et al. 2006) and therefore provide comparative perspective for CMIP3 simulations. For this reason, this study is performed using the following climate models:

- Three DEMETER (Palmer et al. 2004) coupled seasonal forecast models (ECMWF, Météo-France and UK Met Office (UKMO)), which have long hindcasts extending back to mid-20th century, and are analyzed for their El Niño teleconnections. Increasing greenhouse gasses are not specified in these hindcasts, but given the consistency of ENSO at least over the last half of the 20th century (Nicholls 2008) this fact should not be a limiting factor for seasonal forecast models.
- Nine CMIP3 coupled climate change models selected and grouped according to their 20th century ENSO characteristics (based on the analysis of AchutaRao and Sperber 2006):

Too weak ENSO variability: CCCMA; GISS-ER; MIROC-3.2 (med-res)

About right ENSO variability: CCSM3; HADCM3; GFDL-2.0

Too strong ENSO variability: CNRM; ECHAM5; GFDL-2.1

These three groups are hereafter referred to as weak, moderate, and strong, respectively. For

the groups of models labeled moderate and strong according to their reproduction of El Niño variability, most of these models were also deemed as most realistic according to their representation of tropical Pacific climatology (Guilyardi, 2006, 5 out of the 6), and their coupled air-sea variability characteristics (van Oldenborgh et al. 2005a, 4 out of 6).

For the 21st century climate, the A2 Special Report on Emissions Scenario (SRES) projection is chosen for the nine climate change models listed above, as this defines the current worst case envisioned for increased greenhouse gas concentrations. Given that precipitation changes are more subtle than temperature changes, stronger forcing allows for easier detection.

Table 1 provides a list of all coupled climate models and the number of ensemble members for the 20th and 21st centuries used in the study. The 20th century analysis of El Niño teleconnections covers the period from 1959 to 2001, which is the common period of data availability for both seasonal forecast and climate change models. The CRU-UEA TS2.1 (Mitchell and Jones, 2005) is used as the observational precipitation dataset. Both climate model and observed precipitation have been interpolated to a common regular $2.5^{\circ} \times 2.5^{\circ}$ degree grid. The analyses presented here focus on the boreal winter (December-to-February, DJF) season, representing the observed peak season for El Niño, and the boreal summer (June-to-August, JJA) season when El Niño events typically evolve. Because the seasonality often determines the relevance of El Niño impacts, particularly for precipitation, by examining only specific seasons some regional impacts might not be represented within this study.

The analysis focuses on tropical land (30°N to 30°S) and uses a simple meteorological interpretation of drought: below-normal precipitation based on a threshold of seasonally standardized precipitation. No universal definition for drought exists. For agricultural drought, the primary

concern is soil moisture, which is also strongly impacted by evaporation as well as details of snow melt and soil characteristics (e.g. Wang 2005). For hydrological drought, evaporative changes due to temperature are again important as is water demand and even the year-to-year persistence characteristics of the precipitation (e.g. McCabe and Wolock 2007). Even a simple meteorological definition will have its shortcomings. The value of 0.3 standard deviations of the standardized precipitation has been chosen to define the drought threshold because this value approximates the expected standard error following a single-sample z test in a composite of eleven cases (i.e. eleven El Niño events as explained below) drawn from standardized data. Therefore, regions with standardized precipitation anomalies less than or equal to -0.3 are considered to be under drought conditions. The results are consistent using stricter criteria for delimiting drought, which will be illustrated in section 3b when investigating drought spatial extent. Lyon (2004) showed similar consistency in results using differing levels of drought severity.

To investigate tropical droughts associated with El Niño during the 20th century, composites of standardized precipitation anomalies have been constructed (Fig. 1). The observed composite for DJF (Fig. 1a) is given by the mean standardized precipitation anomalies for the eleven years (1963/64, 1965/66, 1968/69, 1972/73, 1977/78, 1982/83, 1986/87, 1987/88, 1991/92, 1994/95 and 1997/98) classified as El Niño events. El Niño classification is determined by the Niño-3.4 index (mean SST anomaly in the equatorial Pacific region between 5°N , 5°S , 120°W , 170°W) falling in the upper quartile of the observed distribution. The Niño-3.4 index is chosen because it is a standard and straightforward measure previously shown to correlate most strongly to remote world-wide climate anomalies (Barnston et al. 1997), which is currently used as the primary measure communicated in ENSO monitoring and prediction. Similarly, the observed composite for the JJA standardized precipitation anomalies also includes eleven years (1963, 1965, 1969, 1972, 1982, 1987, 1991, 1992, 1993, 1994 and 1997). Regions with less than 30 mm seasonal precipitation are

considered to either be deserts or be experiencing the dry season and are masked out. As previously documented (Ropelewski and Halpert 1987; Mason and Goddard 2001), El Niño events typically lead to negative precipitation anomalies during DJF over northern South America and parts of Indonesia, southern Africa and north Australia (Fig. 1a). Indonesia, India, Northern South America and much of Central America experience negative precipitation anomalies during JJA of El Niño events (Fig. 1b).

3. El Niño in the 20th and 21st centuries

For the climate change models, an approach similar to that used for the observational Niño-3.4 data is used to delimit El Niño conditions; the upper quartile of the model Niño-3.4 time series determines the El Niño years in each simulation run (i.e. each ensemble member) of each model after carefully removing the effect of temperature trends in the model projections. The temperature trend effect is minimized by computing anomalies relative to a moving 30-year climatological period preceding the year under consideration, consistent with what might be done in real-time forecasting. The upper quartile of Niño-3.4 index that delimits an El Niño event is determined using the preceding 30-year climatological period. The use of a 30-year periods aligns with the World Meteorological Organization (WMO) recommendation, which currently advises the use of the period from 1971 to 2000 as the climatological period for computing climate anomalies.

The standardized precipitation anomalies incorporating the long term mean and standard deviation have also been produced by computing the climatology from the 30 years of data prior to the year being considered. Figure 2 shows 20th century El Niño standardized precipitation anomaly composites for the 9 CMIP3 models investigated for both DJF (first three rows) and JJA (last three rows). All the weak models (first column) have weak teleconnections and (except CCCMA in JJA) and not statistically significant pattern correlations (Table 2) at the 5% level. Pattern correlation

significance has been tested using 500 random composite samples of eleven 20th century model fields generated using a bootstrap resampling procedure with replacement. The ranked pattern correlations of the 500 composites, computed against the observed composite (Fig. 1), determine the statistical significance. Values of Table 2 falling outside the 95% confidence interval are label as statistically significant at the 5% level.

Among the moderate and strong El Niño models, those that were judged to exhibit realistic SST variability – namely GFDL-2.0, GFDL-2.1, HADCM3, and ECHAM5 (van Oldenborgh et al. 2005a) – all also exhibit the most realistic teleconnections. The El Niño composite precipitation anomalies for these models (except in HADCM3 in JJA) correlate significantly with the observed composite at the 5% level (Table 2). Consistent with the results of Lyon (2004), Fig. 2 shows a clear relationship between the magnitude of regional El Niño precipitation teleconnections and the magnitude of El Niño variability as represented in each group of models. Such a relationship between the strength of El Niño and local precipitation response might be expected in a single model. The existence of this relationship across models highlights the concern for possible increasingly strong El Niño events in the future.

Prior to examining changes in El Niño teleconnections in the 21st century, we first examine changes in El Niño itself. The IPCC (2007) suggests that the models are split in their tendency for more or less El Niño variability in the future, but that the trends in tropical Pacific SST most often correlate positively with El Niño (Meehl et al, 2007, cf. Fig. 10.16). Although this is consistent with the studies cited earlier (van Oldenborgh et al. 2005a; Collins et al. 2005; Merryfield, 2006), the highly condensed nature of the IPCC summary on ENSO falls short in indicating what the models are actually indicating with regard to El Niño, and gives the impression that we will either have more El Niño events in the future, or that trends in the mean climate are likely to reflect persistent El Niño conditions.

To what degree can significant conclusions be drawn on the change in El Niño characteristics from the limited number of cases available for a phenomenon that contains large inter-event variability? Subtle differences leaning towards more or less El Niño variability in the future could be influenced by the period analyzed (Knutson et al. 1997) or by a particular outlier ensemble member. Here, each model's ensemble member is treated individually, as any single ensemble member could represent a realization of nature. Recall that the designation of an El Niño even in the CMIP3 models throughout the last half of the 20th century and through the 21st century rests on the climatology and event thresholds of the previous 30 years.. For each ensemble member of a particular model, the magnitude of El Niño events over the 20th or 21st centuries constitute sample populations that may or may not be drawn from the same distribution. For investigating possible changes in the magnitude of El Niño we apply the Wilcoxon rank sum test (Wilcoxon, 1945), which is equivalent to the Mann-Whitney U-test (Mann and Whitney, 1947) testing the null hypothesis that the two populations are drawn from identical continuous distributions with equal medians. The significance level (p -value) at which the null hypothesis may be rejected is plotted (Fig. 3a) for all possible pairs of DJF ensemble members from the 20th and 21st centuries compared to one another (black diamonds) and between different DJF ensemble members within the 20th century (gray circles). Any point below the 0.05 p -value line indicates that the difference in the medians of the two samples is statistically significant at the 5% level. One must consider the range of values from pairing the different ensemble members within a given century in addition to the few cases suggesting significant differences between the 20th and the 21st centuries. Even within the 20th century, it is possible to show statistically significant differences in the magnitude of El Niño events at the 5% level, though the two runs were subject to identical external forcing. The importance of larger ensemble availability is obvious for both the historical simulations and the future projections, especially for drawing conclusions on changes in variability.

Small ensemble sizes similarly limit examination of change in the frequency of El Niño events, making statistical tests much more difficult. One can get a sense of how El Niño frequency in DJF is projected to change in the models and how the paucity of ensemble members clouds definitive conclusions by simply looking at the number of El Niño events in 50-year chunks within the 20th and 21st centuries (Figure 3b). Six overlapping 50-year chunks were used for each century: 1901-1950, 1911-1960, 1921-1970, 1931-1980, 1941-1990, and 1951-2000, and similarly for the 21st century. For the models that do not contain El Niño events (e.g. GISS-ER), increased frequency results merely from the fact that the tropical Pacific warms due to the external forcing, so going forward SSTs appear increasingly warmer than the previous 30-years. For models that do contain El Niño events, the frequency of events for the 21st century typically resides within the range seen during the 20th century, or approximately 1 event per 4 years. Cases do exist showing frequencies not experienced in the 20th century, but no monotonic increases through the 21st century are found. The importance of multiple ensemble projections is clearly demonstrated by CCSM3, which provides five ensemble members for the 21st century. Quite different conclusions on the future of El Niño frequency could be drawn if one had only the single member that ended the 21st century with unprecedented El Niño frequency compared to the situation in which one had only the single member that ended with a frequency close to the 20th century low. Although some slight tendency towards possible small increases of El Niño frequency can be seen in these models, no robust conclusions can be drawn other than that discerning such a shift in the observed record will defy attribution to global warming. This conclusion indicates that given the limited sampling available from both the observed record and the climate model projections, the characteristics of El Niño events through the 21st century are currently projected to remain consistent with those of the 20th century. Similar conclusions exist for El Niño strength and frequency changes for JJA (not shown).

4. Tropical El Niño teleconnections in the 21st century in coupled model projections

a) Spatial patterns and magnitude

The previous section has shown that the strength of El Niño events is not projected to change in the 21st century. However, the background mean climate against which El Niño events evolve is changing. To what extent will the changes in tropical mean climate modify El Niño teleconnections? And, does the strength or frequency of ENSO variability as represented by a particular model influence the character of the climate change precipitation response in the model?

The results presented in Section 3 show that across climate models, and as previously shown by Lyon (2004) using observations, the strength of tropical precipitation teleconnections scales with the strength of El Niño. Therefore, tropical precipitation will henceforth be further composited across models in the weak, moderate and strong El Niño groups to focus the common features within the groups and highlight differences due to different representation of El Niño (Figs. 4 and 5). The superiority of pattern correlation in the teleconnections among the DEMETER models particularly in DJF (Table 2) is related to a more realistic spatial pattern of El Niño afforded by ocean initialization compared to the free running climate change simulations (Misra et al, 2008), just as within the CMIP3 models, those with more realistic representation of ENSO SST variability contained better representation of the tropical teleconnection patterns. As the magnitude of the El Niño related precipitation anomalies scales with the strength of El Niño, the moderate group yields the most similarity to the seasonal forecast DEMETER composite (Figs. 4b-d and Fig. 5b-d).

Comparison of the 21st century El Niño standardized precipitation anomaly composites (Figs. 4e-g) with the 20th century composites (Figs. 4b-d) for DJF reveals that neither the magnitude of the anomalies nor the spatial patterns are projected to change substantially in the 21st century in any of the three groups of models, despite the fact that the climate mean state changes. Similar results are found for JJA (Fig. 5). Statistical significance of the differences has been assessed by generating

1000 random samples using a simple bootstrap resampling procedure with replacement for each group of models for 20th and 21st centuries. The statistical significance for the difference between the 20th and 21st century composites depends on whether or not the 95% confidence intervals for the 20th and 21st century composites overlap. This procedure has been applied at each grid point independently. For nearly all land areas no differences have been detected at the 5% level. (i.e. no changes have been identified between the 20th and 21st century El Niño composite projections) (not shown). The number of grid points differing at the 5% level or better is less than that expected by chance.

Examination of teleconnection differences in Figures 4 and 5 is based on standardized anomalies. However, there may be changes in precipitation variability (i.e. the standard deviation) that would not appear in the relative standardized precipitation anomalies. Thus the same analysis of changes in El Niño teleconnections is applied to quantitative precipitation anomaly composites. The observed actual precipitation anomaly El Niño composite in $\text{mm}\cdot\text{day}^{-1}$ (Fig. 6a) shows a similar pattern to the observed standardized precipitation anomaly composite (Fig. 1a), as do the model groups (Fig. 6b-g compared to Fig. 4b-d) In accordance with the standardized precipitation anomaly composites (Figs. 4b-g), actual precipitation anomaly composites (Figs. 6b-g) for all three groups of climate change models do not show marked differences between the 20th and 21st century El Niño composite projections. Therefore, both in relative and absolute senses no differences exist between El Niño composite projections for the 20th and 21st centuries. Similar results have been found for JJA (not shown).

b) Range of variability and spatial extent

Figure 7 illustrates, using boxplots (also known as box and whisker diagrams), the range of variability between El Niño composites for all ensemble members of each group of models for four

regions where El Niño events typically lead to reduced precipitation in DJF: a) northern South America (10°N, 10°S, 75°W, 50°W), b) southern Africa (20°S, 30°S, 10°E, 40°E), c) Indonesia (2.5°S, 7.5°S, 110°E, 120°E), and d) North Australia (10°S, 20°S, 130°E, 150°E). The boxplots shown in Fig.7 are constructed using the standardized precipitation anomaly composites.

The central grey box of the DEMETER seasonal forecast model group incorporates the observed standardized precipitation anomaly composite (horizontal dashed line) for northern South America (panel a), southern Africa (panel b) and North Australia regions (panel d). The mean (black dot) and median (thick horizontal line) values for the DEMETER group over these three regions are also close to the observed standardized precipitation anomaly, indicating good performance in predicting the observed standardized precipitation anomaly. Over Indonesia (panel c) the DEMETER group shows a large spread, indicating high prediction uncertainty or large intra-event variability, but the ensemble range of values does contain the observed anomaly. The ensemble range of values for nearly all groups of models shows the ability of these models to cover the observed anomaly during the 20th century. The only two exceptions are the weak group of models for southern Africa (Fig. 7b) and the moderate group of models for Indonesia (Fig. 7c), where the range of the ensemble does not cover the observed value. The comparison of the boxplots for each group of climate change models shows a consistent overlap between the range of values projected for the 20th and 21st centuries. In accordance with Fig. 4 this result supports the finding of no discernable change between the 20th and 21st century El Niño projections for northern South America, southern Africa, Indonesia and north Australia.

Figure 8 shows El Niño standardized precipitation anomaly composite boxplots for three regions where El Niño leads to reduced precipitation in JJA: a) northern South America (10°N, 10°S, 75°W, 50°W), b) Indonesia (2.5°S, 7.5°S, 110°E, 120°E), and c) East Australia (20°S, 30°S, 140°E, 150°E).

Overall, the same features described above for DJF are present in JJA. The main difference compared to DJF is the larger number of model groups with the ensemble range of values unable to cover the observed anomaly during the 20th century (e.g. the DEMETER and weak group of models for South America (Fig. 8a) and the weak, moderate and strong group of models for Indonesia (Fig. 8b)).

Another important El Niño feature is the spatial extent of the precipitation anomaly, particularly negative ones (Fig. 9). Boxplots are constructed for all ensemble members available for each group of models. The DEMETER, weak and moderate model groups have mean (black dot) and median (thick horizontal line) close to the observed fraction (horizontal dashed line) during the 20th century, indicating that these two model groups have a good spatial extent of negative anomalies during El Niño years. Ensemble members from the strong El Niño models show a higher fraction of grid points with drought during El Niño than seen in the weak and moderate models. Only DEMETER and weak models do contain the observed fraction within their ensemble range during the 20th century in DJF (Fig. 9a,b), while for JJA the DEMETER, weak and moderate models do contain the observed fraction (Fig. 9c,d). All three groups of climate change models suggest a slight reduction in the spatial extent of drought, at both severity levels, compared to the 20th century projected fraction. However, the 21st century results are based on far fewer ensemble members than used for the 20th century. This sampling issue and the amount of overlap between the two centuries mean that the result of a slight reduction should be interpreted with caution.

5. El Niño-induced drought risk: The intersection between climate variability and change

The climate literature states that climate change projections for many parts of the world depend on how ENSO may change in the future (van Oldenborgh et al. 2005a). Projections have even been called into question because of the limited ability of most climate change models to represent

ENSO. Thus, a reasonable question would be: To what extent does the fidelity of ENSO in a coupled model influence the resulting changes in the mean climate? For the tropics, broadly, the ability of a model to represent the dominant aspect of climate variability, namely ENSO, does not control the climate change response. Figure 10 shows the projected change, between the periods 2071-2100 and 1971-2000, in the mean DJF and JJA precipitation from the three climate change model groups. Consistent with the tendency towards a warmer tropics in the 21st century (IPCC 2007) all three climate change model groups project increases in tropical precipitation, particularly between 10°N and 10°S (e.g. Held and Soden 2006). The magnitude and broad pattern of the projected precipitation change do not scale with the strength of ENSO in the models. The differences between models within any particular group (not shown) are typically larger than the differences between the groups shown in Figure 10. Thus changes in mean precipitation within the tropics are largely independent of a model's ENSO characteristics. Even models that have little to none ENSO variability (Figs. 10a and 10d) produce a change in mean precipitation of similar magnitude and spatial structure to those models with exceedingly strong ENSO variability (Figs. 10c and 10f).

The intersection of projected changes in mean precipitation and projected El Niño precipitation teleconnections for the 21st century can help identify regions where adverse El Niño-related precipitation impacts are likely to decrease or increase in the future. The results presented so far provide supportive evidence that for the tropics, climate variability and change are largely separable. Therefore, it may be possible to combine, or layer, information from the different timescales (i.e. long term climate change and short term climate variability) obtained from different sources. In terms of climate variability, the models project unchanging precipitation teleconnections associated with ENSO. However, that variability is riding on top of a changing mean climate that is attributable to anthropogenic climate change. This means that even if the climate variability is

unchanged, the risks of a predefined event such as drought (i.e. precipitation below a certain value) will change.

A distinction exists between a set of predictions that robustly suggests no change and a set of predictions for which large differences among the models lead to an average neutrality projection. Unfortunately, in the use of multi-models for climate change, similar information typically results from both situations; a net prediction of no change implies conditions of the past persist into the future. Both situations exist in this analysis. For climate variability, the set of models consistently indicates no significant change in El Niño strength or magnitude. Further, the models predict no change in the precipitation teleconnections associated with El Niño events. Thus, the observed El Niño teleconnections of the 20th century can be used to represent those of the 21st century. However, climate variability exists in combination with a changing mean climate. For the change in mean climate the models do not always agree at local to regional scales. The main difficulty in dealing with the situation of diverging model predictions is: Which models should one trust? If the models were all equally credible, the spread of predictions should contribute to estimating the probabilistic uncertainty of the outcome. The approach taken by the IPCC AR4 (Meehl et al, 2007) is simply to form multi-model averages, and possibly to highlight areas where the models agree in the magnitude, or at least the sign, of their 21st century climate change. Similar approaches are adopted here to examine the changing risk of drought, or more specifically deficient precipitation.

The threshold for drought conditions is defined to be the 30th percentile of the observed precipitation distribution for the last half of the 20th century, based on a fit of the observed values at each point to a gamma distribution. For standardized normally distributed data, the 30th percentile coincides approximately with 0.5 standard deviations below average. This threshold is not necessarily the relevant measure of drought for all locations, and as mentioned earlier,

consideration of only precipitation ignores other variables relevant to drought such as temperature. This example merely illustrates how changing risk of some predetermined quantitative threshold could be assessed with the data available. By construction, the risk of “drought” over the last half of the 20th century is 30%. The quantitative value of how much precipitation is associated with the 30th percentile will vary spatially. In the example shown in Fig. 11, the threshold for drought is approximately 75 mm of rainfall for the season. To produce probabilistic maps of drought risk during El Niño conditions in the 20th century, just those eleven observations associated with El Niño conditions are used to fit a gamma distribution. The resulting cumulative distribution function (CDF) permits estimation of the probability of the pre-defined threshold. In the example (Fig. 11), risk of falling below the drought threshold (75 mm) increases to about 50% during El Niño conditions, or an increase in drought risk of about 20% compared to the 20th century climatological risk. Maps of these probabilities during El Niño conditions for DJF and JJA in the 20th century reiterate the known teleconnection regions (Figs. 12a and 13a). Masked out regions (Figs. 12a, 13a, and left-hand panels in Figs. 12b-e and 13b-e) indicate climatologically dry areas according to the mean precipitation of the 20th century as described in Section 2.

The risk of drought during El Niño conditions near the end of the 21st century is obtained by layering the climate information of variability and change (Figs. 12b and 13b). The change in mean precipitation is determined from the climate change models by differencing the (1971-2000) and (2071-2100) multi-model mean. The precipitation change is then added to the observed time series, the parameters of the gamma distributions are recalculated, and the probabilities for the pre-defined threshold are re-evaluated. Addition of the projected change effectively shifts the CDF based on the sign of the change. In the example (Fig. 11), the precipitation change is negative, and the probability for receiving less than 75 mm for the season increases climatologically to about 60% and to about 80% during El Niño conditions at the end of the 21st century, which translates into a

30% increase in drought risk.

The question of confidence in the multi-model mean precipitation changes remains. A number of criteria are considered to illustrate the sensitivity of the results to how one determines confidence. If confidence cannot be established at a location, the assumption is that the mean precipitation change cannot be determined, and no change is imposed on the characteristics of the 20th century timeseries for use in calculating 21st century risk probabilities. In those cases, the drought risk probabilities remain unchanged in the left hand panels compared to Figs. 12a and 13a, and the grid box is masked out in the maps of change in risk (e.g. Figs. 12c-e and 13c-e, right hand side). The first case uses the multi-model mean as is (Figs. 12b and 13b), assuming all models are equally plausible and considers the multi-model average as the best guess for the change. The second case considers model agreement (Figs. 12c and 13c), assuming that if the majority of the models agree in their sign of the change, the multi-model mean change is more reliable. Agreement among 80% of the models (or 7 out of 9) is required, following similar analyses in the IPCC AR4. The third case more stringently requires that the multi-model mean must exceed the spread of the models (Figs. 12d and 13d), estimated by the standard deviation of the 9 model values. The final case includes only those models with realistic ENSO variability (ECHAM5, GFDL2.0, GFDL2.1, HADCM3) according to van Oldenbourg et al. (2005a). In this final case, it is further required that at least 3 of the 4 models share the same sign of precipitation change.

The change in risk of crossing the predefined drought threshold changes similarly in the multi-model mean and the four models that reproduce realistic ENSO characteristics. However, the four models with reasonable ENSO fidelity show greater agreement among themselves and also indicate enhanced risk of drought over some of the aforementioned teleconnection regions, which seems to be only weakly shared by the other models. The significance of this finding has not been

established given that this result was obtained using only 4 models. Further, it has yet to be demonstrated that fidelity of climate variability in a model portends better fidelity in the forced climate change response. More important than the specific values of this analysis, however, is the example of putting the information together and the implications for confidence in the modification of climate risk depending on how one employs the climate change projection information.

6. Conclusions

This study has investigated El Niño-induced tropical droughts (in the meteorological sense, i.e. precipitation deficit) in climate change projections. Initially, diagnostics based on the projected Niño-3.4 index assessed how ENSO will behave in the 21st century. Next, the spatial pattern, magnitude, range of variability and spatial extent of El Niño-induced deficit precipitation patterns in both 20th and 21st centuries was examined. Finally, a procedure for combining climate variability with change information for producing El Niño-induced drought risk estimates for the 21st century was illustrated. The main findings for the mature (DJF) and development (JJA) stages of El Niño can be summarized as follows:

- No significant change in relative El Niño strength or robust change in frequency is noted between climate change model simulations for the 20th and 21st centuries. Based on an analysis that considers the intra-ensemble variability from individual models, any observed shift in ENSO characteristics will be effectively impossible to attribute to global warming.
- Climate change models that do simulate ENSO variability appropriately exhibit realistic El Niño-induced drought patterns in the 20th century, and those are not projected to change in the 21st century due to global warming. To our knowledge, this is the first report on how El Niño-induced tropical drought patterns are projected to appear in the 21st century. Remarkably, these models produce tropical teleconnections almost as well as seasonal prediction models. Droughts

observed during El Niño years in northern South America, and parts of southern Africa, Indonesia, India and Australia are consistently well reproduced by these models. The fact that both ENSO variability and the magnitude of the precipitation response remain unchanged suggests a fairly linear separation between timescales. The implications for such a separation, particularly in the context of climate risk management and climate change adaptation, are substantial.

- Furthermore, precipitation changes projected for the 21st century by all climate change model groups here investigated show consistency and qualitative robustness, independent of the ability of these models to simulate ENSO variability in the tropical Pacific. All three model groups project increase in tropical precipitation, particularly between 10°N and 10°S, supporting the separability between climate change and ENSO-like climate variability in the tropics.
- The spatial extent of El Niño-induced tropical droughts over land at different levels of severity is projected to be slightly reduced in the 21st century by all climate change models when compared to the spatial extent projected for the 20th century.
- The fact that El Niño-induced tropical drought patterns are not projected to change in the 21st century supports the use of the observed El Niño teleconnections in the 20th century to represent future climate conditions in the 21st century. Because the mean climate is projected to change in the 20th century, even if the climate variability relative to the mean climate is unchanged, the risks of a predefined event such as drought will change. A procedure for combining El Niño climate variability and projected changes in mean precipitation for the 21st century for estimating future drought risk for a predefined drought threshold has been illustrated. Increased risk has been found in some regions for those models that do show good fidelity in reproducing ENSO variability in the 20th century. These changes are not an artifact of increasing or reducing ENSO variability, as it was these models that indicated no statistically robust change in El Niño characteristics. There is, however, no study to date demonstrating a coincidence between the

quality of a model's representation of climate variability and change.

Acknowledgements

This research has been funded by U.S. CLIVAR DRought In COupled Models Project (DRICOMP). CASC was supported by Fundacao de Amparo a Pesquisa do Estado de Sao Paulo (FAPESP), processes 2005/05210-7 and 2006/02497-6. LG was supported in part under cooperative agreement NA05OAR4311004 between Columbia University and the National Oceanic and Atmospheric Association. We thank the EU-funded DEMETER project for making their multi-model seasonal hindcasts available at the ECMWF public data server. We also acknowledge the IPCC modeling groups, the Program for Climate Model Diagnosis and Intercomparison (PCMDI) and the WCRP's Working Group on Coupled Modeling (WGCM) for their roles in making available the WCRP CMIP3 multi-model dataset. Support of this dataset is provided by the Office of Science, U.S. Department of Energy.

References

AchutaRao, K. and K. R. Sperber, 2006: ENSO simulation in coupled ocean-atmosphere models: Are the current models better? *Clim. Dyn.*, DOI 10.1007/s00382-006-0119-7.

Barnston, A.G, M. Chelliah, and S.B. Goldenberg, 1997: Documentation of a highly ENSO-related SST region in the equatorial Pacific. *Atmos-Ocean*, 35, 367-383.

Clement, A. C., R. Seager, M. A. Cane, and S. E. Zebiak, 1996: An ocean dynamical thermostat, *J. Clim.*, 9, 2190–2196.

Coelho C.A.S., D. B. Stephenson, M. Balmaseda, F. J. Doblas-Reyes and G. J. van Oldenborgh, 2006: Towards an integrated seasonal forecasting system for South America. *J. Climate*. Vol. 19, No. 15, 3704-3721.

Collins, M. and The CMIP Modelling Groups, 2005: El Niño- or La Niña-like climate change? *Clim. Dyn.*, 24, 89-104

Dilley, M., R. S. Chen, U. Deichmann, A. L. Lerner-Lam, and M. Arnold. 2005: *Natural Disaster Hotspots: A Global Risk Analysis*. Washington, D.C.: World Bank, 145pp.

Easterling, D.R, T.W.R. Wallis, J.H. Lawrimore, R.R. Heim, Jr, 2007: Effects of temperature and precipitation trends on U.S. drought. *Geophys. Res. Lett.*, 34, L20709, doi:10.1029/2007GL031541.

Guilyardi, E., 2006: El Niño – mean state – seasonal cycle interactions in a multi-model study. *Clim. Dyn.*, 26, 329-348.

Held, I.M. and B.J. Soden, 2006: Robust responses of the hydrological cycle to global warming. *J. Climate*, 19, 5686-5699.

Hoerling, M., and J. Eischeid, 2007: Past peak water in the Southwest, *Southwest Hydrol.*, 6, 18.

IPCC, 2007: *Climate Change 2007: The Physical Science Basis. Contribution of Working Group I to the Fourth Assessment Report of the Intergovernmental Panel on Climate Change* [Solomon, S., D. Qin, M. Manning, Z. Chen, M. Marquis, K.B. Averyt, M. Tignor and H.L. Miller (eds.)]. Cambridge University Press, Cambridge, United Kingdom and New York, NY, USA, 996 pp.

Knutson, T.R., S. Manabe, and D. Gu, 1997: Simulated ENSO in a global couple ocean-atmosphere model: Multidecadal amplitude modulation and CO₂ sensitivity. *J. Climate*, 10, 138-161.

Lyon, B., 2004: The strength of El Niño and the spatial extent of tropical drought. *Geophys. Res. Lett.*, 31, L21204, doi: 10.1029/2004GL020901.

Mann, H. B. and D. R. Whitney, 1947: On a test of whether one of two random variables is stochastically larger than the other. *Annals of Mathematical Statistics*, 18, 50-60.

Mason, S.J. and L. Goddard, 2001: Probabilistic precipitation anomalies associated with ENSO. *Bull. Amer. Met. Soc.*, 82, 619-638.

McCabe, G.J. and D.M. Wolock, 2007: Warming may create substantial water supply shortages in the Colorado River basin. *Geophys. Res. Lett.*, 34, L22708, doi:10.1029/2007GL031764

Meehl, G.A. and co-authors, 2007: Global Climate Projections. In: *Climate Change 2007: The Physical Science Basis. Contribution of Working Group I to the Fourth Assessment Report of the Intergovernmental Panel on Climate Change* [Solomon, S., D. Qin, M. Manning, Z. Chen, M. Marquis, K.B. Averyt, M. Tignor and H.L. Miller (eds.)]. Cambridge University Press, Cambridge, United Kingdom and New York, NY, USA.

Merryfield, W., 2006: Changes to ENSO under CO₂ doubling in a multimodel ensemble. *J. Climate*, 19, 4009-4027.

Misra V, L. Marx, M. Fennessey, B. Kirtman and J. Kinter, 2008. A comparison of climate prediction and simulation over the Tropical Pacific, *J. Climate*, 21, 3601-3611.

Mitchell, T. D. and P. D. Jones, 2005: An improved method of constructing a database of monthly climate observations and associated high-resolution grids. *Int. J. Climatol.*, 25, 693-712.

Neelin, J. D., C. Chou, and H. Su, 2003: Tropical drought regions in global warming and El Niño teleconnections. *Geophys. Res. Lett.*, 30, L2275, doi:10.1029/2003GL018625.

Nicholls, N., 2008: Recent trends in the seasonal and temporal behaviour of the El Niño – Southern Oscillation. *Geophys. Res. Lett.* 35, L19703, doi:10.1029/2008GL034499.

Nohara, D., A. Kitoh, M. Hosaka, and T. Oki, 2006: Impact of climate change on river discharge projected by multi-model ensemble. *J. Hydromet.*, 7(5), 1076-1089.

Palmer, T.N., A. Alessandri, U. Andersen, P. Cantelaube, M. Davey, P. Délecluse, M. Déqué, E. Díez, F.J. Doblas-Reyes, H. Feddersen, R. Graham, S. Gualdi, J.-F. Guérémy, R. Hagedorn, M. Hoshen, N. Keenlyside, M. Latif, A. Lazar, E. Maisonave, V. Marletto, A. P. Morse, B. Orfila, P. Rogel, J.-M. Terres, M. C. Thomson, 2004: Development of a European multi-model ensemble system for seasonal to inter-annual prediction (DEMETER). *Bulletin of the American Meteorological Society*, 85, 853-872.

Ropelewski, C. F. and M. S. Halpert, 1987: Global and Regional Scale Precipitation Patterns Associated with the El Niño/Southern Oscillation. *Mon. Wea. Rev.*, 115, 1606-1626.

Sterl, A., G. J. van Oldenborgh, W. Hazeleger and G. Burgers, 2007: On the robustness of ENSO teleconnections. *Clim. Dyn.*, 29, 469–485.

van Oldenborgh, G.J., S.Y. Phillip and M. Collins, 2005a: El Niño in a changing climate: A multi-model study. *Ocean Sci*, 1, 81-95.

van Oldenborgh, G. J., M. A. Balmaseda, L. Ferranti, T. N. Stockdale and D. L. T. Anderson, 2005b: Evaluation of atmospheric fields from the ECMWF seasonal forecasts over a 15- year period. *J. Climate*, 18, 3250–3269.

Vecchi, G.A., A. Clement, and B. J. Soden, 2008: Examining the Tropical Pacific's response to global warming. *EOS*, 89, 81-83.

Wang, G., 2005: Agricultural drought in a future climate: results from 15 global climate models participating in the IPCC 4th assessment. *Clim. Dyn.*, 25, 739-753, DOI 10.1007/s00382-005-0057-9.

Wilcoxon, F., 1945: Individual comparisons by ranking methods. *Biometrics Bulletin*, 1, 80-83.

List of figures

Figure 1: Observed standardized anomaly El Niño composites for the 20th Century. a) DJF composite . b) JJA composite.

Figure 2: Standardized anomaly El Niño composites for the 20th Century for the nine coupled climate change models investigated. Weak models for DJF (Panels a-c). Moderate models for DJF (Panels g-i). Strong models for DJF (Panels m-o). Weak models for JJA (Panels d-f). Moderate models for JJA (Panels j-l). Strong models for JJA (Panels p-r).

Figure 3: Robustness of changes in El Niño magnitude and frequency. (a) Significance level (i.e. p-value) of Wilcoxon Rank Sum test for DJF Niño 3.4 index equal medians comparing all possible pairs of samples from individual ensemble members of El Niño magnitude within the 20th century (grey circles) and between the 20th and 21st centuries (black diamonds, median value marked with larger diamond); (b) Frequency of El Niño events within 50-year periods during the 20th century (open diamonds) and 21st century (black stars). See text for additional information. Final 50-year period of 21st century highlighted with black squares.

Figure 4: DJF standardized precipitation anomaly El Niño composites for the DEMETER group (panel a), weak group (panel b), moderate group (panel c) and strong group (panel d) during the 20th century. Panels e-g show standardized precipitation anomaly El Niño composites for the weak, moderate and strong groups during the 21st century, respectively.

Figure 5: JJA standardized precipitation anomaly El Niño composites for the DEMETER group (panel a), weak group (panel b), moderate group (panel c) and strong group (panel d) during the 20th

century. Panels e-g show standardized precipitation anomaly El Niño composites for the weak, moderate and strong groups during the 21st century, respectively.

Figure 6: Observed DJF precipitation anomaly El Niño composite (panel a). Panels b-d show DJF precipitation anomaly El Niño composites for the weak, moderate and strong groups during the 20th century, respectively. Panels e-g show DJF precipitation anomaly El Niño composites for the weak, moderate and strong groups during the 21st century, respectively. Precipitation anomalies are expressed in $\text{mm}\cdot\text{day}^{-1}$.

Figure 7: Boxplots of DJF El Niño composites standardized precipitation anomaly for all ensemble members available for the four groups of models investigated. Boxplots are shown for four regions: a) northern South America (10°N , 10°S , 75°W , 50°W), b) southern Africa (20°S , 30°S , 10°E , 40°E), c) Indonesia (2.5°S , 7.5°S , 110°E , 120°E), and d) North Australia (10°S , 20°S , 130°E , 150°E). Boxplots located to the left (right) of the vertical dotted line are for the 20th (21st) century composites. The horizontal dashed line is the observed composite standardized precipitation anomaly in the 20th century. The central horizontal thick line within the box is the median value among all ensemble members. The box represents the inter-quartile range. The whiskers are drawn as far as the highest and lowest values of the ensemble. The black dot is the ensemble mean.

Figure 8: Boxplots of JJA El Niño composites standardized precipitation anomaly for all ensemble members available for the four groups of models investigated. Boxplots are shown for four regions: a) northern South America (10°N , 10°S , 75°W , 50°W), b) Indonesia (2.5°S , 7.5°S , 110°E , 120°E), and c) East Australia (20°S , 30°S , 140°E , 150°E). Boxplots located to the left (right) of the vertical dotted line are for the 20th (21st) century composites. The horizontal dashed line is the observed composite standardized precipitation anomaly in the 20th century. See text for additional

explanation.

Figure 9: Boxplots for the fraction of land grid points with negative standardized precipitation anomaly El Niño composites for the four groups of models investigated for two drought severity levels: DJF (panel a) and JJA (panel c) standardized precipitation anomalies less than 0.3, and DJF (panel b) and JJA (panel d) standardized precipitation anomalies less than 0.5. Boxplots are constructed using the grid point fraction of negative standardized precipitation anomaly composites for all ensemble members for each group of models. Boxplots located to the left of the vertical dotted line are for the 20th century composites. Boxplots located to the right of the vertical dotted line are for the 21st century composites. The horizontal dashed line is the observed fraction of land grid points with negative standardized precipitation anomaly El Niño composite in the 20th century.

Figure 10: Difference in DJF (panels a, b and c) and JJA (panels d, e and f) mean precipitation anomaly (in $\text{mm}\cdot\text{day}^{-1}$) between the period 2071-2100 and 1971-2000 simulated by weak (first row), moderate (second row) and strong (third row) El Niño groups of climate change models.

Figure 11: Cumulative distribution functions for precipitation showing the probability (%) of receiving less than a given amount of precipitation (mm) based on fitting a gamma distribution to observed values at a single grid point. The CDFs for 20th century precipitation (solid lines) are drawn both for all years (grey: DJF 1959-2001) and El Niño conditions during that period. Similar curves are presented for the 21st century precipitation by added the CMIP3 multi-model mean precipitation changes to the observed 20th century timeseries and re-estimating the parameters.

Figure 12: Risk of deficient precipitation, defined as the 30th percentile of the observed 20th century distribution, during El Niño conditions for DJF (a) during the period 1959-2001; (b) during 2071-

2100, based on the multi-model mean (MMM), lhs, and the difference (b,left)-(a) on rhs; (c) similar to (b) but only considering MMM when 7 of the 9 models agree in sign; (d) similar to (b) but only considering MMM when that value exceeds the standard deviation of the 9 models at that point; (e) similar to (b) but only considering the 4 models deemed to have realistic ENSO variability according to van Oldenborgh et al. (2005) and additionally requiring that 3 of the 4 models agree in sign of the precipitation change. White areas in (a) and left-hand panels indicate 20th century mean precipitation is less than 30mm for the season. Additional white areas in right-hand panels indicate low confidence in precipitation change, or effectively no ability to predict change in El Niño related drought risk there.

Figure 13: Same as figure 12, for JJA.

Table 1: Coupled climate models and number of ensemble members for the 20th and 21st century simulations used in this study.

Modeling group	Acronym	20 th century members	21 st century members
European Centre for Medium-range Weather Forecasts	ECMWF	9	-
Centre National de Recherches Météorologiques	Météo-France	9	-
United Kingdom Meteorological Office	UKMO	9	-
	DEMETER group	27	-
Center for Climate System Research (The University of Tokyo), National Institute for Environmental Studies, and Frontier Research Center for Global Change (JAMSTEC)	MIROC3.2(medres)	3	3
Canadian Centre for Climate Modeling and Analysis	CCCMA	5	5
Goddard Institute for Space Studies (NASA)	GISS-ER	9	1
	Weak group	17	9
National Center for Atmospheric Research	CCSM3	8	5
Geophysical Fluid Dynamics Laboratory (NOAA)	GFDL-2.0	3	1
Hadley Centre for Climate Prediction and Research (Met Office)	HADCM3	2	1
	Moderate group	13	7
Centre National de Recherches Météorologiques (Météo-France)	CNRM	1	1
Max Plank Institute for Meteorology	ECHAM5	4	3
Geophysical Fluid Dynamics Laboratory (NOAA)	GFDL-2.1	3	1
	Strong group	8	5

Table 2: Standardized anomaly El Niño composite pattern correlation for the 20th century. The symbol * indicates statistically significant pattern correlation at the 5% level. See text for additional explanation.

Acronym	DJF	JJA
ECMWF	0.62*	0.43*
Météo-France	0.51*	0.44*
UKMO	0.64*	0.48*
DEMETER group	0.69*	0.50*
MIROC3.2(medres)	0.25	0.33
CCCMA	0.29	0.25*
GISS-ER	0.22	0.17
Weak group	0.36*	0.30*
CCSM3	0.15	0.33*
GFDL-2.0	0.57*	0.42*
HADCM3	0.46*	0.28
Moderate group	0.38*	0.42*
CNRM	0.23*	0.35*
ECHAM5	0.50*	0.48*
GFDL-2.1	0.54*	0.49*
Strong group	0.60*	0.54*

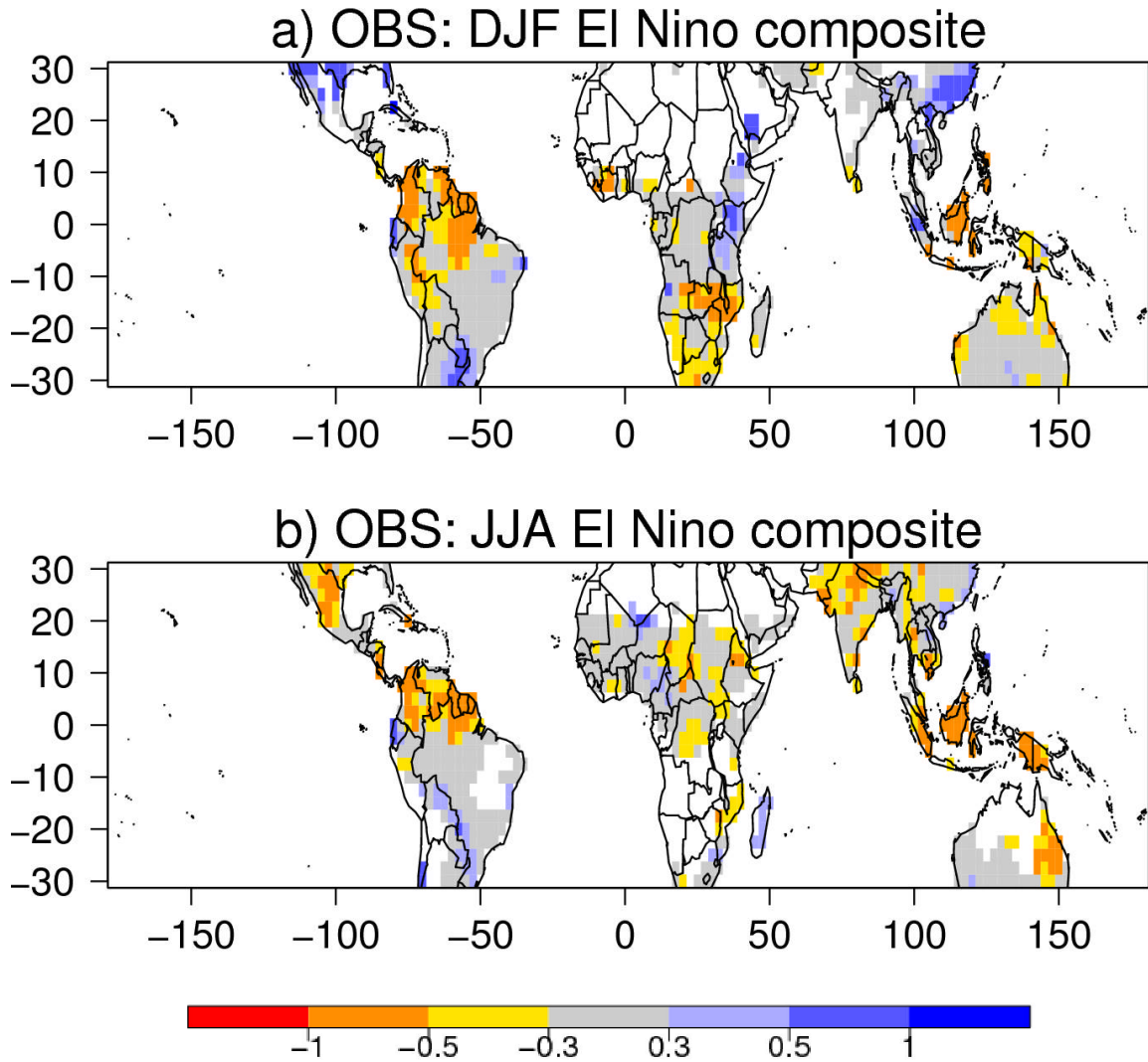


Figure 1: Observed standardized anomaly El Niño composites for the 20th Century. a) DJF composite . b) JJA composite.

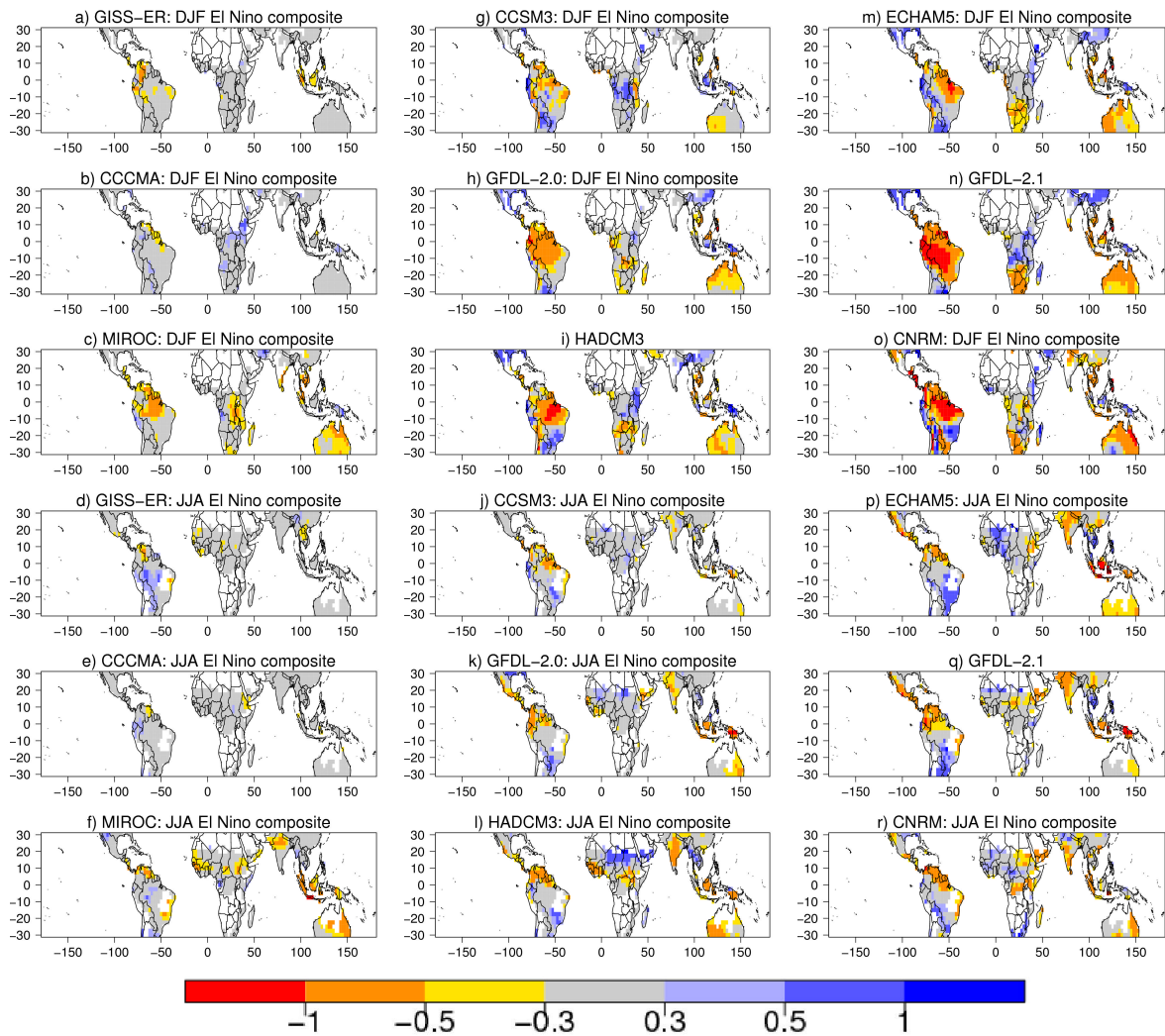


Figure 2: Standardized anomaly El Niño composites for the 20th Century for the nine coupled climate change models investigated. Weak models for DJF (Panels a-c). Moderate models for DJF (Panels g-i). Strong models for DJF (Panels m-o). Weak models for JJA (Panels d-f). Moderate models for JJA (Panels j-l). Strong models for JJA (Panels p-r).

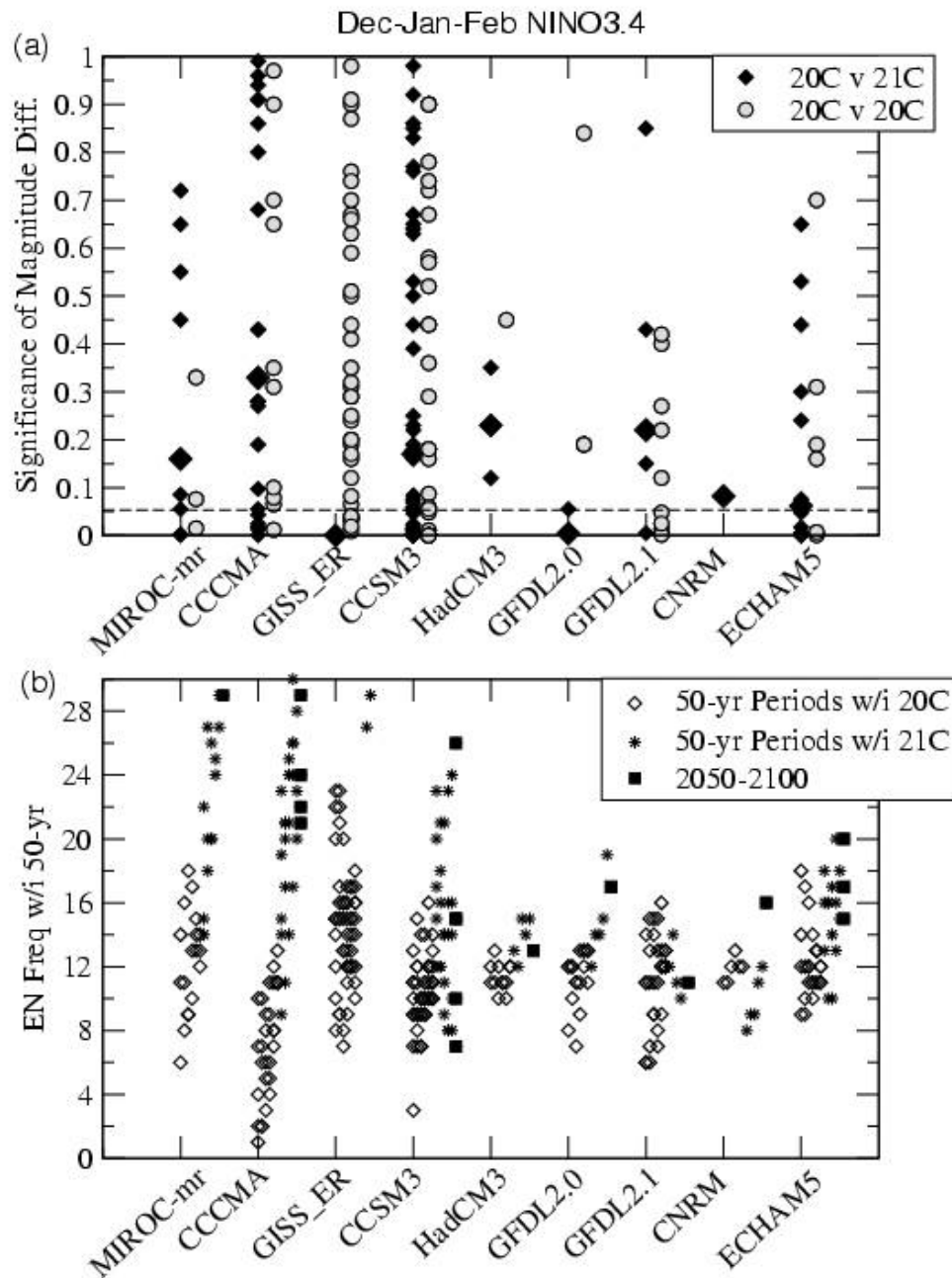


Figure 3: Robustness of changes in El Niño magnitude and frequency. (a) Significance level (i.e. p-value) of Wilcoxon Rank Sum test for DJF Niño 3.4 index equal medians comparing all possible pairs of samples from individual ensemble members of El Niño magnitude within the 20th century (grey circles) and between the 20th and 21st centuries (black diamonds, median value marked with larger diamond); (b) Frequency of El Niño events within 50-year periods during the 20th century (open diamonds) and 21st century (black stars). See text for additional information. Final 50-year period of 21st century highlighted with black squares.

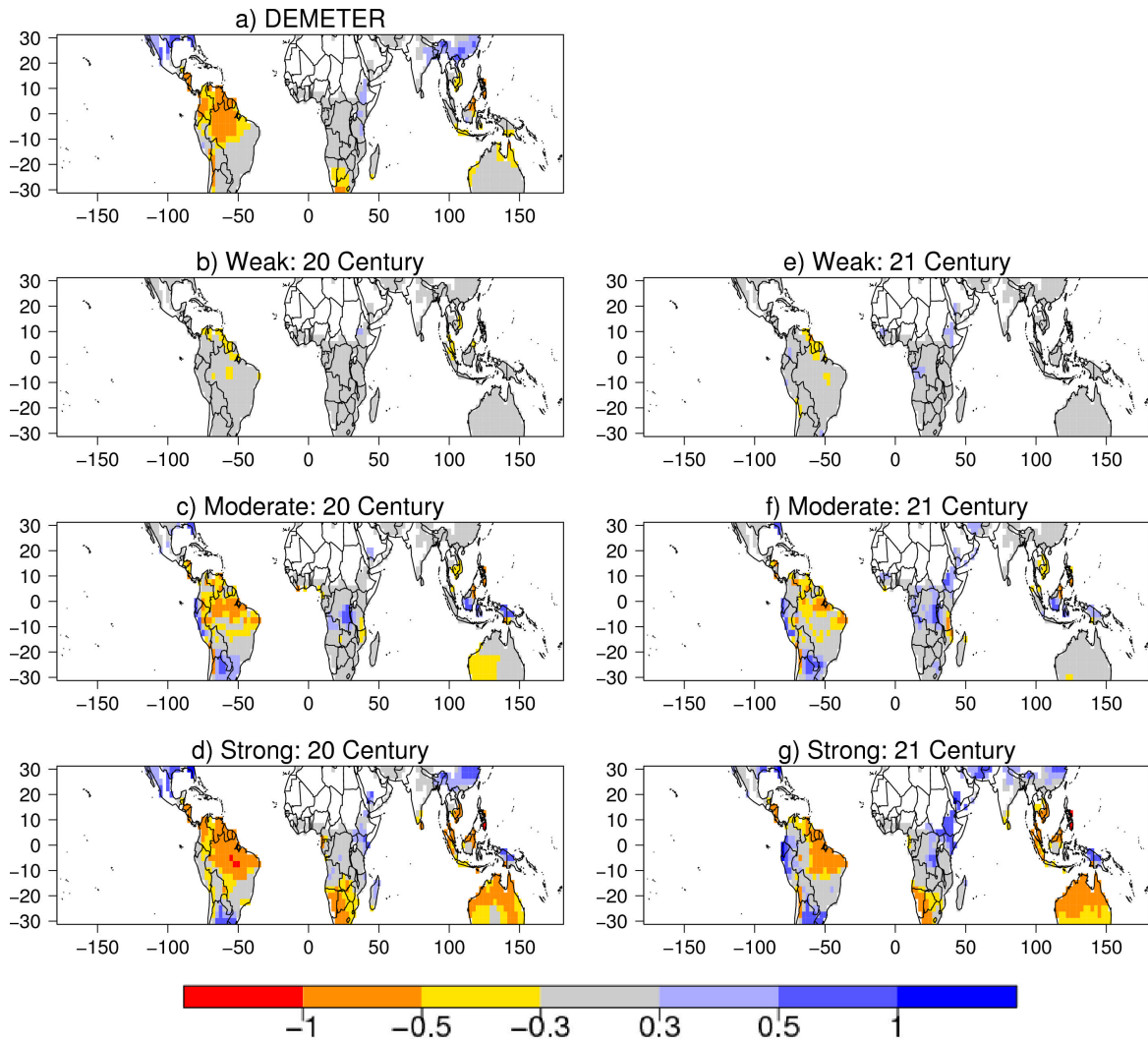


Figure 4: DJF standardized precipitation anomaly El Niño composites for the DEMETER group (panel a), weak group (panel b), moderate group (panel c) and strong group (panel d) during the 20th century. Panels e-g show standardized precipitation anomaly El Niño composites for the weak, moderate and strong groups during the 21st century, respectively.

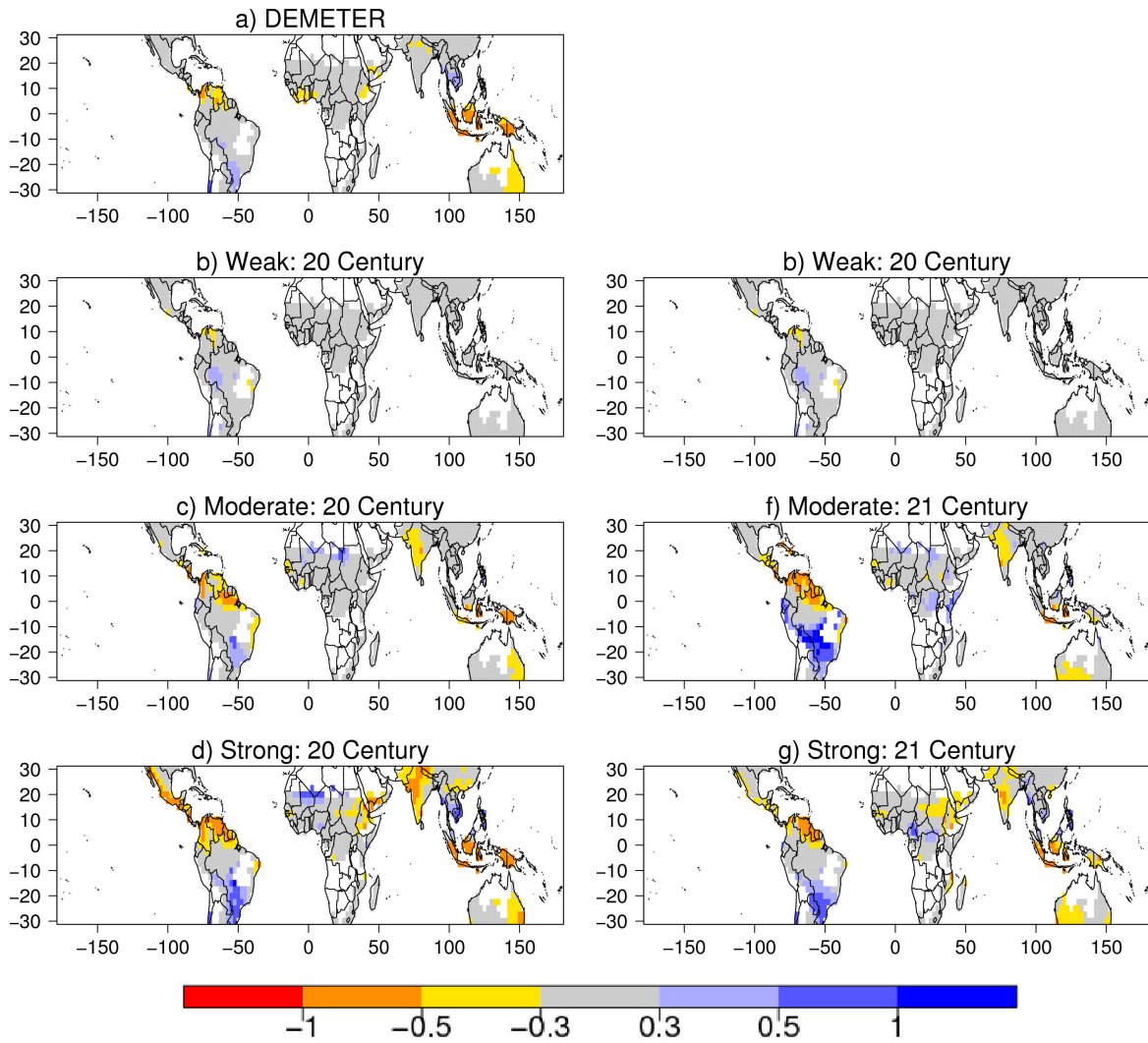


Figure 5: JJA standardized precipitation anomaly El Niño composites for the DEMETER group (panel a), weak group (panel b), moderate group (panel c) and strong group (panel d) during the 20th century. Panels e-g show standardized precipitation anomaly El Niño composites for the weak, moderate and strong groups during the 21st century, respectively.

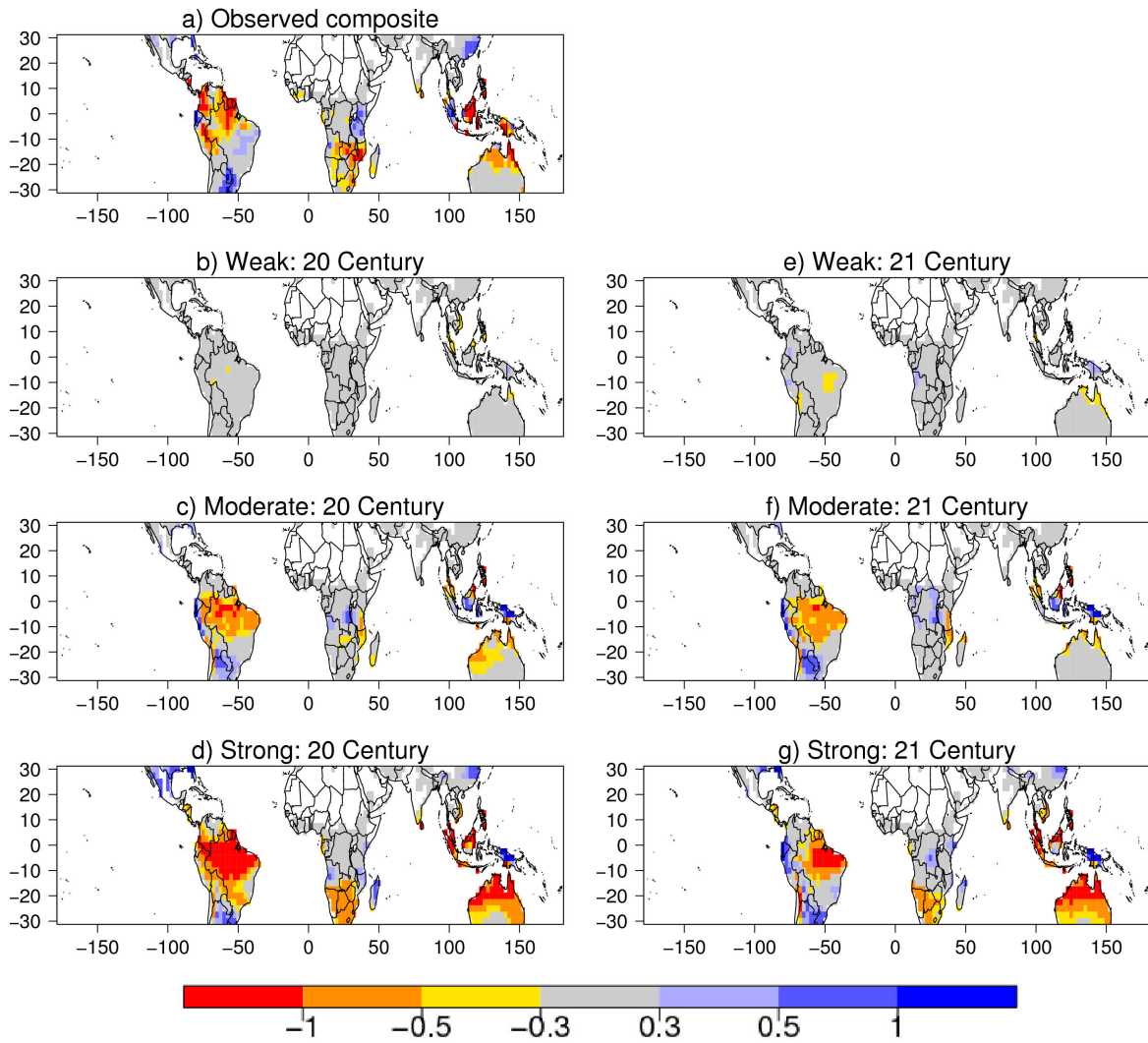


Figure 6: Observed DJF precipitation anomaly El Niño composite (panel a). Panels b-d show DJF precipitation anomaly El Niño composites for the weak, moderate and strong groups during the 20th century, respectively. Panels e-g show DJF precipitation anomaly El Niño composites for the weak, moderate and strong groups during the 21st century, respectively. Precipitation anomalies are expressed in mm.day⁻¹.

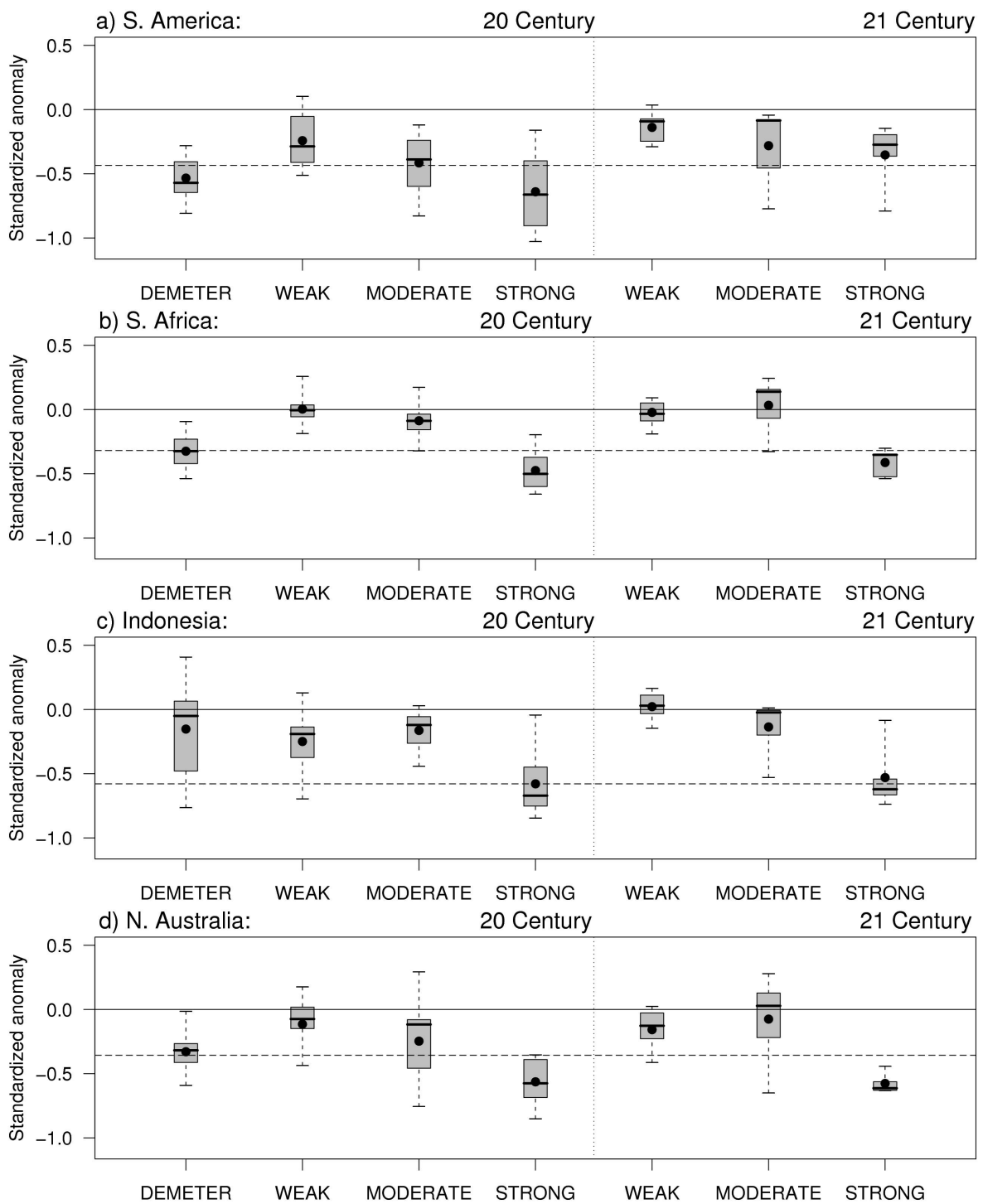


Figure 7: Boxplots of DJF El Niño composites standardized precipitation anomaly for all ensemble members available for the four groups of models investigated. Boxplots are shown for four regions: a) northern South America (10°N, 10°S, 75°W, 50°W), b) southern Africa (20°S, 30°S, 10°E, 40°E), c) Indonesia (2.5°S, 7.5°S, 110°E, 120°E), and d) North Australia (10°S, 20°S, 130°E, 150°E). Boxplots located to the left (right) of the vertical dotted line are for the 20th (21st) century composites. The horizontal dashed line is the observed composite standardized precipitation anomaly in the 20th century. See text for additional explanation.

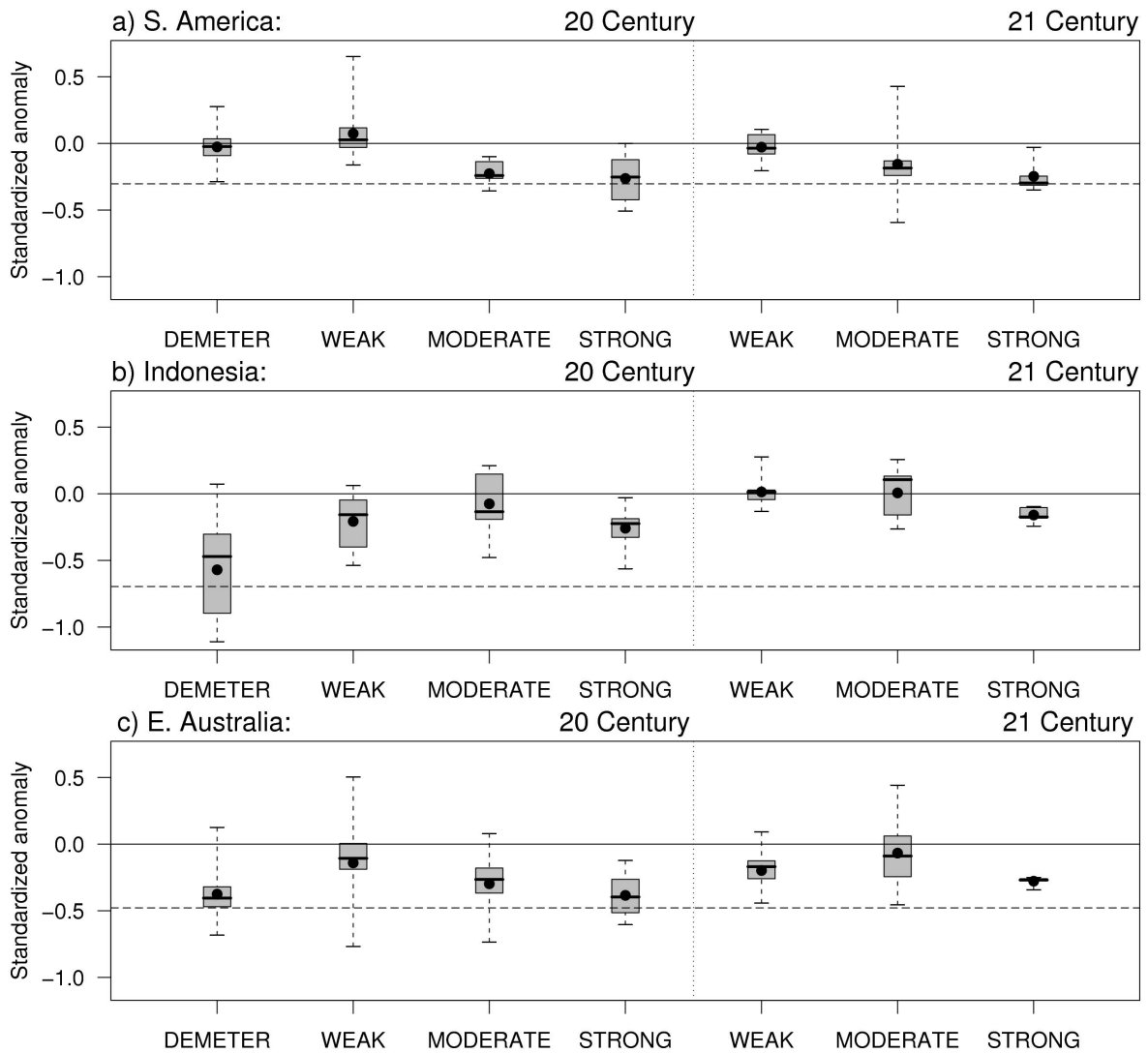


Figure 8: Boxplots of JJA El Niño composites standardized precipitation anomaly for all ensemble members available for the four groups of models investigated. Boxplots are shown for four regions: a) northern South America (10°N , 10°S , 75°W , 50°W), b) Indonesia (2.5°S , 7.5°S , 110°E , 120°E), and c) East Australia (20°S , 30°S , 140°E , 150°E). Boxplots located to the left (right) of the vertical dotted line are for the 20th (21st) century composites. The horizontal dashed line is the observed composite standardized precipitation anomaly in the 20th century. See text for additional explanation.

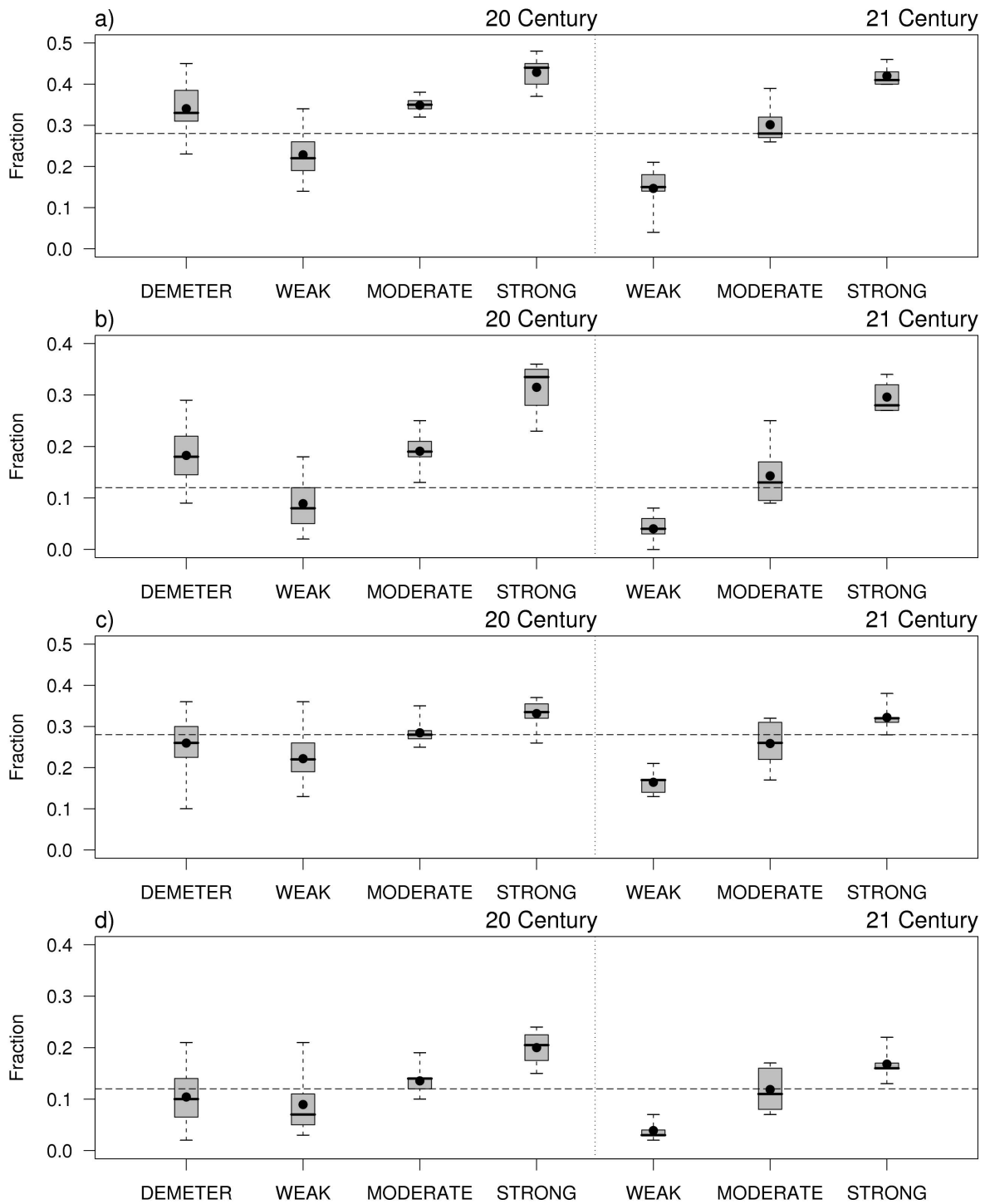


Figure 9: Boxplots for the fraction of land grid points with negative standardized precipitation anomaly El Niño composites for the four groups of models investigated for two drought severity levels: DJF (panel a) and JJA (panel c) standardized precipitation anomalies less than 0.3, and DJF (panel b) and JJA (panel d) standardized precipitation anomalies less than 0.5. Boxplots are constructed using the grid point fraction of negative standardized precipitation anomaly composites for all ensemble members for each group of models. Boxplots located to the left of the vertical dotted line are for the 20th century composites. Boxplots located to the right of the vertical

line are for the 21st century composites. The horizontal dashed line is the observed fraction of land grid points with negative standardized precipitation anomaly El Niño composite in the 20th century.

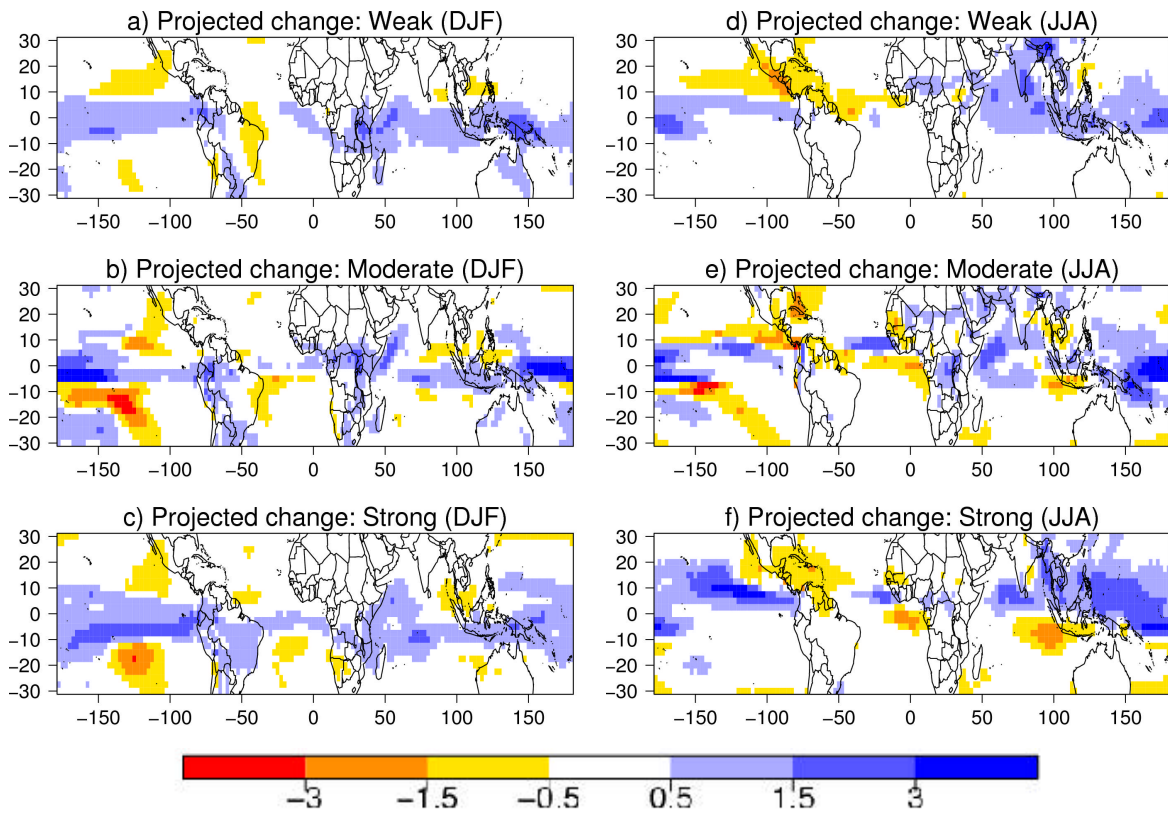


Figure 10: Difference in DJF (panels a, b and c) and JJA (panels d, e and f) mean precipitation anomaly (in $\text{mm}\cdot\text{day}^{-1}$) between the period 2071-2100 and 1971-2000 simulated by weak (first row), moderate (second row) and strong (third row) El Niño groups of climate change models.

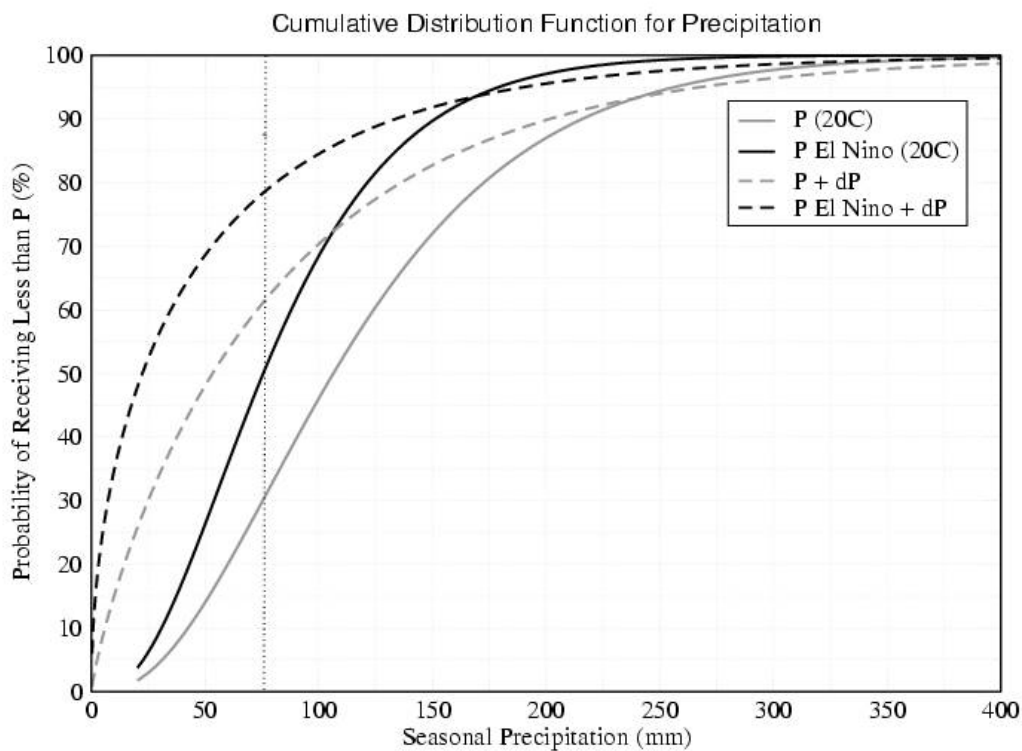


Figure 11: Cumulative distribution functions for precipitation showing the probability (%) of receiving less than a given amount of precipitation (mm) based on fitting a gamma distribution to observed values at a single grid point. The CDFs for 20th century precipitation (solid lines) are drawn both for all years (grey: DJF 1959-2001) and El Niño conditions during that period. Similar curves are presented for the 21st century precipitation by added the CMIP3 multi-model mean precipitation changes to the observed 20th century timeseries and re-estimating the parameters.

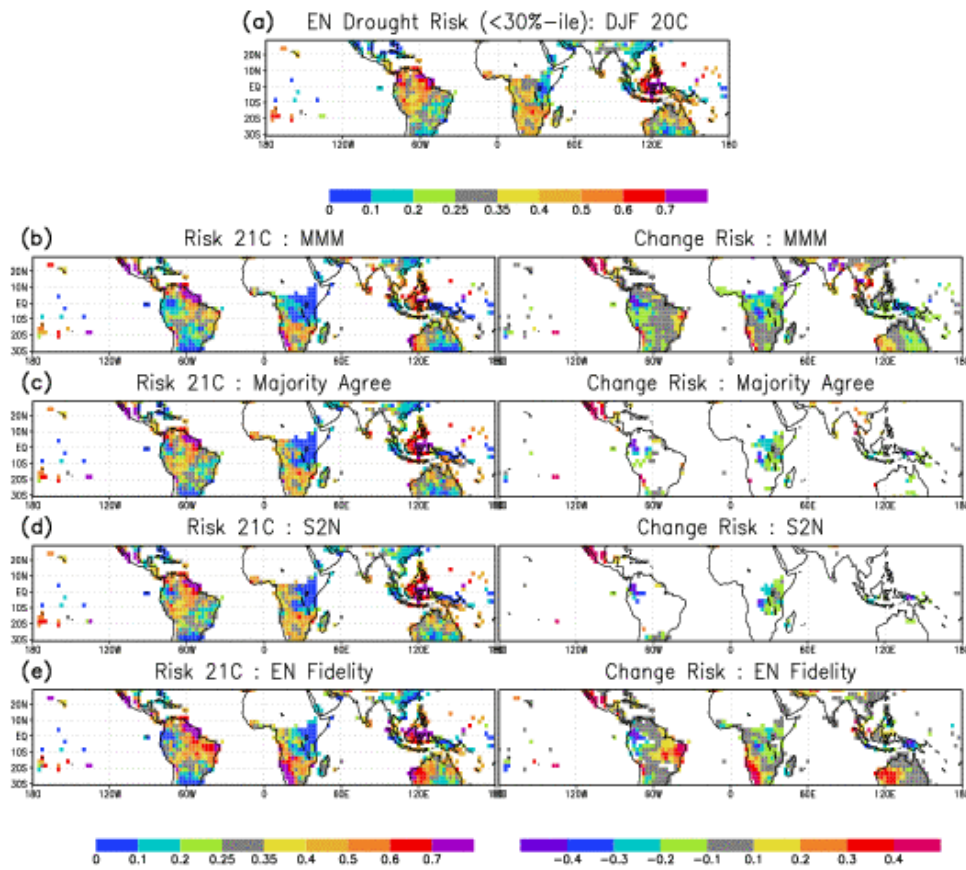


Figure 12: Risk of deficient precipitation, defined as the 30th percentile of the observed 20th century distribution, during El Niño conditions for DJF (a) during the period 1959-2001; (b) during 2071-2100, based on the multi-model mean (MMM), lhs, and the difference (b,left)-(a) on rhs; (c) similar to (b) but only considering MMM when 7 of the 9 models agree in sign; (d) similar to (b) but only considering MMM when that value exceeds the standard deviation of the 9 models at that point; (e) similar to (b) but only considering the 4 models deemed to have realistic ENSO variability according to van Oldenborgh et al. (2005) and additionally requiring that 3 of the 4 models agree in sign of the precipitation change. White areas in (a) and left-hand panels indicate 20th century mean precipitation is less than 30mm for the season. Additional white areas in right-hand panels indicate low confidence in precipitation change, or effectively no ability to predict change in El Niño related drought risk there.

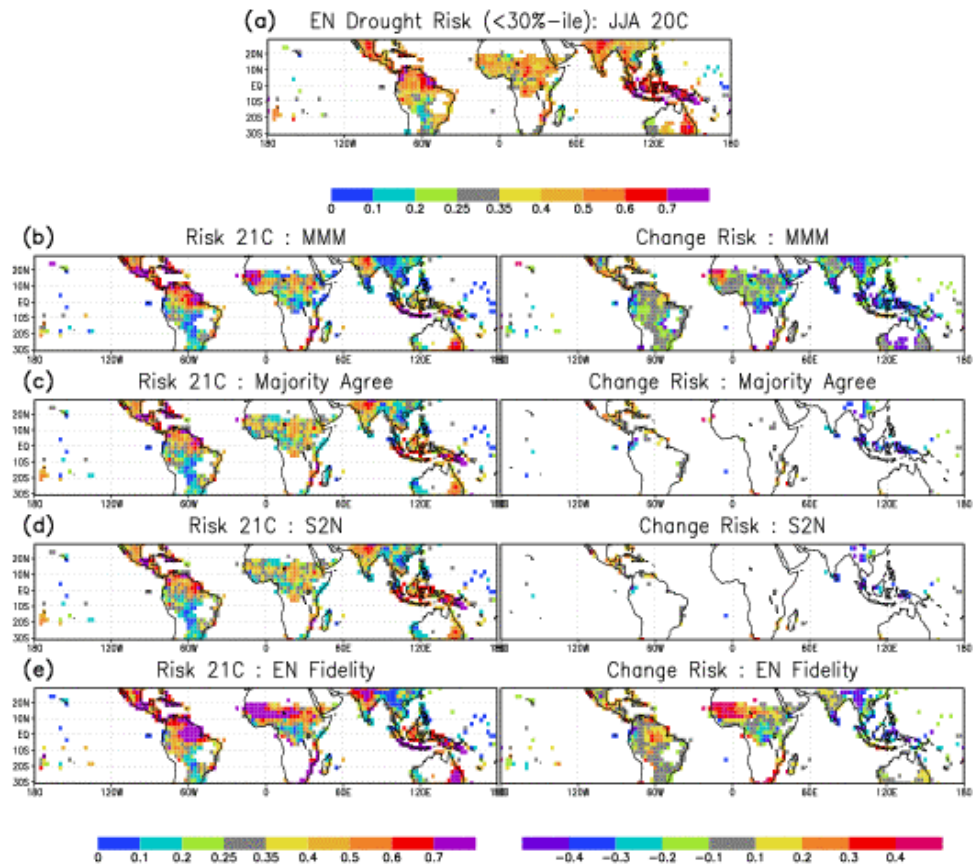


Figure 13: Same as figure 12, for JJA.